Receptor-type guanylyl cyclases confer thermosensory responses in *C. elegans*

Asuka Takeishi[1,3], Yanxun V. Yu[1,3], Vera M. Hapiak[1], Harold W. Bell[1], Timothy O'Leary[2] and Piali Sengupta[1,4]

[1]Department of Biology and National Center for Behavioral Genomics, Brandeis University, Waltham, MA

[2]Department of Engineering, University of Cambridge, Cambridge, United Kingdom

[3]Equal contributions listed alphabetically

[4]Corresponding author: sengupta@brandeis.edu

SUMMARY

Thermosensation is critical for optimal regulation of physiology and behavior. *C. elegans* acclimates to its cultivation temperature (T_c), and exhibits thermosensitive behaviors at temperatures relative to T_c. These behaviors are mediated primarily by the AFD sensory neurons which are extraordinarily thermosensitive, and respond to thermal fluctuations at temperatures above a T_c-determined threshold. Although cGMP signaling is necessary for thermotransduction, the thermosensors in AFD are unknown. Here we show that AFD-specific receptor guanylyl cyclases (rGCs) are instructive for thermosensation. In addition to being necessary for thermotransduction, ectopic expression of these rGCs confers highly temperature-dependent responses onto diverse cell types. We find that the temperature response threshold is determined by the rGC and cellular context, and that multiple domains contribute to their thermosensory properties. Identification of thermosensory rGCs in *C. elegans* provides insight into mechanisms of thermosensation and thermal acclimation, and suggests that rGCs may represent a new family of molecular thermosensors.

INTRODUCTION

Detection of temperature by dedicated thermosensory circuits allows animals to seek optimal thermal conditions for survival and reproduction, and to avoid noxious heat or cold (Terrien et al., 2011). Although members of the conserved transient receptor potential (TRP) family of cation channels mediate thermosensation in multiple metazoans (Barbagallo and Garrity, 2015; Vriens et al., 2014), whether proteins other than TRP channels also act as thermosensors in diverse species remains to be fully determined.

C. elegans acclimates to its cultivation temperature (T_c), and exhibits distinct thermotaxis strategies in physiological temperature ranges relative to T_c (Hedgecock and Russell, 1975). Behavioral acclimation to T_c is reflected in part by adaptation of the thermosensory response threshold (T^*_{AFD}) of the bilateral AFD sensory neuron pair (Biron et al., 2006; Clark et al., 2006; Kimura et al., 2004; Mori and Ohshima, 1995; Ramot et al., 2008; Yu et al., 2014). Measurements of intracellular calcium dynamics and temperature-evoked currents have shown that AFD depolarizes and hyperpolarizes upon warming and cooling, respectively, at temperatures warmer than T^*_{AFD} to drive thermotaxis behaviors (Clark et al., 2006; Kimura et al., 2004; Ramot et al., 2008). Thermosensory responses and T^*_{AFD} adaptation appear to be cell-intrinsic properties although AFD response dynamics can be further shaped by surrounding glial cells (Kobayashi et al., 2016; Yoshida et al., 2015). However, despite extensive characterization of thermosensation in *C. elegans*, the molecular nature of thermosensor(s) in AFD remains unidentified.

Several lines of evidence suggest that thermosensation in AFD is unlikely to be mediated by thermosensitive ion channels. AFD exhibits a steep temperature dependence

with a reported Q_{10} of $>10^{15}$ for temperature-evoked current, implying a strong amplification step in the thermotransduction process (Ramot et al., 2008). Moreover, a ~100 ms latency has been observed between changes in the temperature stimulus and evoked current suggesting the involvement of a second messenger in thermosensory signaling (Ramot et al., 2008). Genetic and behavioral experiments suggest that this second messenger is cGMP. AFD neurons in animals mutant for AFD-specific receptor guanylyl cyclases (AFD-rGCs), or cGMP-gated channels, fail to respond to temperature changes, and these animals are behaviorally atactic on thermal gradients (Garrity et al., 2010). Based on these observations, we and others have proposed that warming increases and/or decreases the catalytic activity of rGCs or phosphodiesterases (PDEs), respectively, and that the resulting increase in intracellular cGMP activates cyclic nucleotide-gated channels to depolarize AFD (Garrity et al., 2010). However, whether rGCs or PDEs are themselves thermosensors, or act downstream of other thermosensory proteins in AFD is unknown.

Here we show that a set of AFD-rGCs is both necessary in AFD for thermosensation, and sufficient to confer robust temperature responses upon expression in diverse non-thermosensory neuronal and non-neuronal cell types. The operating range of AFD-rGC expressing cells is determined largely by the individual rGC and cell type, indicating that T_c-correlated adaptation of thermosensory response threshold is an AFD-specific property. We find that co-expression of AFD-rGCs can further shape temperature responses, and that both the extra-and intracellular domains of these rGCs are necessary for their thermosensitive properties. Identification of thermosensitive rGCs in *C. elegans* provides insight into the mechanisms by which neurons can achieve exceptional

thermosensitivity, and together with the recently identified mouse receptor guanylyl cyclase G thermosensory molecule (Chao et al., 2015), may define a new family of evolutionarily conserved thermoreceptors.

RESULTS

AFD-rGCs are necessary for thermotransduction in AFD

The *gcy-8, gcy-18* and *gcy-23*-encoded rGCs are expressed specifically in AFD, and are localized to the specialized AFD sensory endings (Inada et al., 2006; Nguyen et al., 2014). Temperature-evoked currents in AFD are abolished in animals triply mutant for *gcy-8, gcy-18* and *gcy-23* (Ramot et al., 2008), indicating that these rGCs together are necessary for thermotransduction. While animals singly or doubly mutant for AFD-rGCs have been shown to exhibit thermotaxis behavioral defects (Inada et al., 2006; Wang et al., 2013; Wasserman et al., 2011), the contribution of each rGC to thermotransduction in AFD has not been examined systematically.

To address this issue, we examined temperature-evoked changes in intracellular calcium dynamics in AFD expressing the genetically encoded calcium sensor cameleon YC3.6. As reported previously, wild-type AFD responded robustly to temperature changes at temperatures warmer than T^*_{AFD} (Clark et al., 2006; Kimura et al., 2004) (Figure 1A, Figure S1A, Table S1). These responses were abolished in *gcy-23(nj37) gcy-8(oy44) gcy-18(nj38)* triple mutants (Figure S1A), confirming that loss of function of all three AFD-rGCs abolishes AFD thermotransduction.

We next examined temperature responses in AFD in animals mutant for individual rGCs. We noted that while the *gcy-8(oy44)* and *gcy-18(nj38)* alleles used in

previous studies are likely to be functionally null, *gcy-23(nj37)* is an in-frame deletion predicted to encode a protein that retains the intracellular cyclase domain (Inada et al., 2006) (Figure S1B), and thus may retain partial catalytic function. We, therefore, obtained putative null alleles of *gcy-23* by CRISPR/Cas9-mediated gene editing (Figure S1B). Unlike in triple mutant animals, AFD retained the ability to respond to a rising temperature stimulus in animals mutant for individual AFD-rGC genes (Figure 1A), including in animals carrying any *gcy-23* allele (Figure S1C). AFD also responded robustly to a rising temperature ramp in animals doubly mutant for all three combinations of *gcy* genes, although response amplitudes were variable (Figure 1A). However, consistent with our previous observations (Wasserman et al., 2011), T^*_{AFD} was significantly lower in animals mutant for *gcy-8* (Figure 1B, Table S1), as well as in animals lacking any two of the three AFD-rGC proteins (Wasserman et al., 2011) (Figure 1B, Table S1). We conclude that any one of these AFD-rGCs is sufficient to mediate temperature responses in AFD, but that all three proteins contribute to correct T_c-correlated adaptation of T^*_{AFD}, and appropriate thermotaxis behavior.

Ectopic expression of three AFD-rGCs together is sufficient to confer highly sensitive thermosensory responses onto chemosensory neurons

To determine whether AFD-rGCs are sufficient to confer thermosensory responses onto non-thermosensory cells, we misexpressed all three AFD-rGCs together in the bilateral ASE or AWB chemosensory neuron pairs expressing GCaMP, and quantified temperature-evoked changes in intracellular calcium dynamics. Both ASE and AWB express multiple rGCs that are necessary and partly sufficient for their

chemosensory response profiles, as well as the TAX-2/TAX-4 cGMP-gated channels necessary to mediate chemo- and thermotransduction (Bargmann, 2006; Hobert, 2013). Neither ASE nor AWB responded to warming in wild-type animals (Figure 2A-B), indicating that the rGCs expressed endogenously in these neuron types do not confer temperature responses under the examined conditions, and that the TAX-2/TAX-4 channels are not intrinsically temperature-gated (Ramot et al., 2008).

Remarkably, we found that ectopic expression of all three AFD-rGCs was sufficient to confer robust temperature responses in both the left and right ASE, as well as in both AWB neurons (Figure 2A-B, Movie S1). As in AFD, temperature responses in AFD-rGC expressing AWB neurons were abolished in *tax-4* mutants (Figure 2B). Ectopic thermosensory responses in AWB were unaffected in *gcy-23 gcy-8 gcy-18* triple mutants (Figure 2B), indicating that the observed temperature responses in AWB are independent of thermotransduction in AFD. Compared to AFD, the thresholds (T^*) of temperature-evoked calcium transients in ASE (T^*_{ASE}) and AWB (T^*_{AWB}) expressing AFD-rGCs were modulated to a lesser extent by T_c (Table S1). We conclude that AFD-rGCs are together sufficient to confer temperature responses onto chemosensory neurons, but that the observed T_c-dependent adaptation of T^* is largely an AFD-specific property.

We next quantified the sensitivity of AFD-rGC-conferred temperature responses via measurement of the Q_{10} of temperature-evoked GCaMP fluorescence changes in response to temperature steps of different sizes (Figure 2C). This aggregate Q_{10} measurement reports the temperature-dependence of the rGC enzyme, the endogenous calcium dynamics of each cell type, and the fluorescence change of GCaMP. The mean estimated Q_{10} in AFD was ~193 (Figure 2C) consistent with the previously reported steep

temperature dependence of AFD responses (Ramot et al., 2008). AWB neurons misexpressing AFD-rGCs also exhibited steep, albeit smaller, temperature-dependent changes in fluorescence with a mean Q_{10} of ~53 (Figure 2C). In contrast, AWB neurons expressing GCaMP alone yielded a temperature insensitive response with a Q_{10} of ~1 (Figure 2C). We infer that AFD-rGCs confer a high thermal sensitivity upon misexpression, but that additional AFD-specific properties likely contribute to the thermosensitivity of this neuron type.

Expression of thermoTRP channels in non-thermosensory neurons can modulate neuronal excitability in response to temperature changes and drive behavior (Bernstein et al., 2012). We asked whether temperature-mediated activation of AFD-rGCs misexpressed in AWB is sufficient to alter AWB-mediated behaviors. The AWB neurons mediate avoidance of repellents partly via modulation of turning frequency on odorant gradients (Ha et al., 2010; Tsalik and Hobert, 2003). We maintained control and transgenic animals expressing all three AFD-rGCs in AWB at a constant temperature of 15°C, or subjected them to a rising temperature ramp from 15-28°C that spanned T^*_{AWB} (~22°C), and quantified the number of high angle turns. The number of high angle turns exhibited by control and transgenic animals maintained at 15°C were comparable, and decreased over time as reported previously (Gray et al., 2005; Hills et al., 2004) (Figure 2D). However, transgenic animals turned significantly more than control animals when the temperature of the assay plate rose above T^*_{AWB} (Figure 2D). Turn numbers of transgenic animals were comparable to those of control animals when warmed to noxious temperatures (>27°C) (Figure 2D). These results suggest that temperature-dependent activation of AWB neurons misexpressing AFD-rGCs is sufficient to alter behavior.

Ectopic expression of GCY-23 alone confers thermosensory responses in the physiological temperature range in chemosensory neurons

We next asked whether each AFD-rGC alone is sufficient to confer thermosensitivity upon ectopic expression. We found that misexpression of GCY-23 alone, but not GCY-8 or GCY-18, conferred thermosensitivity onto AWB and ASE in response to a warming ramp in the physiological temperature range of 13-25°C (Figure 3A-B, Movie S2). T^*_{AWB} did not correlate with mCherry expression driven from a *gcy-23::SL2::mCherry* operon in AWB (Figure S2A), suggesting that GCY-23 expression levels do not determine T^*_{AWB}. T^*_{AWB} and T^*_{ASE} were only weakly T_c-dependent (Table S1). These observations suggest that GCY-23 is the primary contributor to temperature responses in AWB and ASE under these conditions.

To confirm that the catalytic activity of GCY-23 is required for its thermosensory properties, we examined responses conferred upon ectopic expression of a mutant GCY-23 protein in which a conserved Asp927 residue in the cyclase domain critical for catalytic functions was mutated to alanine (Liu et al., 1997; Tang et al., 1995; Thompson and Garbers, 1995). Ectopic expression of GCY-23(D927A) in AWB failed to elicit temperature-evoked responses (Figure 3B). Importantly, all three AFD-rGCs, as well as GCY-23(D927A) tagged with GFP were enriched at the distal dendritic tips in AWB (Figure 3C), similar to the localization pattern of these rGCs in AFD (Nguyen et al., 2014). We conclude that thermosensitive responses conferred by GCY-23 require its cyclase activity.

A subset of *C. elegans* rGCs has been proposed to be active as heterodimers due to the absence of residues critical for catalytic functions in individual subunits (Morton, 2004). Although individual AFD-rGCs appear to contain all residues required for catalytic activity, we nevertheless asked whether GCY-23-mediated temperature responses are modified upon coexpression of either GCY-8 or GCY-18. Expression of GCY-8 or GCY-18 together with GCY-23 in AWB did not alter the temperature responses conferred by GCY-23 alone at any T_c, although T^*_{AWB} was slightly increased upon co-expression of GCY-18 (Figure S2B-C, S2F, Table S1). These observations imply that GCY-23 may not heteromerize with either GCY-8 or GCY-18 under these conditions, or that the response properties of these complexes are similar to those conferred upon expression of GCY-23 alone.

GCY-23 confers thermosensitivity upon ectopic expression in muscle

We next examined whether ectopic expression of AFD-rGCs is sufficient to confer thermosensitivity onto non-neuronal tissues. Imaging of intracellular calcium dynamics upon expression of GCaMP in the vulval muscles of *C. elegans* hermaphrodites showed only infrequent temperature responses upon stimulation with a warming ramp, indicating that these tissues are not thermosensitive (Figure 3D, Figure S3). However, we observed robust fluorescence changes in vulval muscles misexpressing GCY-23, but not GCY-18, together with TAX-2/TAX-4 (Figure 3D, Figure S3, Movie S3). Unlike in ASE or AWB, response amplitudes and dynamics were highly variable in vulval muscles (Figure 3D, Figure S3) possibly due to variability in expression levels or subcellular localization of the ectopically expressed cGMP-gated channels, or the absence of glia-

dependent modulation of response dynamics (Yoshida et al., 2015). The threshold of temperature-induced activity in vulval muscles (T^*_{VM}) was ~14°C upon ectopic expression of GCY-23 in animals grown at 20°C (Table S1), further indicating that the T^* for GCY-23-dependent calcium signals is cell type-specific. Only sporadic responses were observed in vulval muscles misexpressing TAX-2/TAX-4 alone, or GCY-23 in the absence of TAX-2/TAX-4 (Figure 3D, Figure S3). We infer that GCY-23 is sufficient to confer thermosensitivity onto non-neuronal tissues in *C. elegans*.

Ectopic expression of GCY-18 confers temperature responses in the noxious range in chemosensory neurons

Since AFD has also been shown to respond to noxious temperatures (Liu et al., 2012), we considered the possibility that unlike GCY-23, GCY-8 and GCY-18 may be activated in non-physiological temperature ranges upon ectopic expression in chemosensory neurons. To test this hypothesis, we examined intracellular calcium dynamics in AWB and ASE neurons misexpressing each rGC individually in response to a warming ramp from 20°C-30°C. While we observed the expected GCY-23-conferred response at ~21.0°C (Figure 4A), AWB and ASE neurons expressing GCY-18 but not GCY-8 exhibited an increase in fluorescence upon warming above 28°C (Figure 4A, Table S1). We confirmed this GCY-18-dependent temperature response by further examining calcium dynamics in AWB neurons expressing GCY-18 in response to a warming ramp from 23°C-33°C (Figure 4B). This response was TAX-4-dependent (Figure 4B). mCherry expression levels driven from a *gcy-18::SL2::mCherry* operon in AWB did not correlate with T^*_{AWB} (Figure S2A), and T^*_{AWB} of GCY-18-misexpressing

neurons was weakly regulated by T_c (Table S1). These results indicate that GCY-18 is sufficient to confer thermosensitivity in a noxious temperature range, upon misexpression in AWB and ASE.

We asked whether coexpression of GCY-8 or GCY-23 modifies the temperature response conferred by GCY-18 in AWB. AWB neurons expressing GCY-8 and GCY-18 retained the ability to respond at warmer temperatures, although T^*_{AWB} was significantly lower (Figure S2D-F, Table S1). However, while co-expression of GCY-18 and GCY-23 in AWB resulted in the expected GCY-23-mediated response at ~21°C, the GCY-18-conferred response at ~28°C was no longer observed (Figure S2D). To exclude possible inhibition of the GCY-18-dependent temperature response by the GCY-23-dependent response at lower temperatures, we grew animals expressing GCY-18 and GCY-23 singly or together at 25°C and stimulated them with a warming ramp from 23°C-33°C. Under these conditions, whereas no response was observed in cells expressing GCY-23 alone, GCY-18 alone conferred a robust response at ~ 28°C (Figure 4C, Figure S2F, Table S1). Neurons coexpressing GCY-18 and GCY-23 exhibited broader and flatter responses than those expressing GCY-18 alone (Figure 4C, Figure S2F, Table S1), suggesting that coexpression of GCY-23 modifies GCY-18-dependent temperature responses in AWB in a complex manner. Together, these results indicate that when expressed individually in AWB, GCY-23 and GCY-18 confer temperature responses in physiological and noxious temperature ranges, respectively, but that coexpression of rGCs can further sculpt temperature responses under specific conditions.

Multiple domains may contribute to the thermosensory properties of rGCs

We next investigated the domains necessary for the ability of AFD-rGCs to confer thermosensation. Phylogenetic analyses suggest that AFD-rGCs are more closely related to each other than to other *C. elegans* rGCs (Inada et al., 2006; Ortiz et al., 2006). We first created chimeric proteins containing different domain combinations of GCY-23 and GCY-1, an rGC required for ASER-mediated responses to a subset of salt ions (Ortiz et al., 2009; Smith et al., 2013) (Figure S4A), and examined temperature-dependent calcium dynamics in ASER neurons misexpressing these proteins. Although all GFP-tagged chimeras were enriched at the dendritic ends of ASE similar to full-length GCY-23 (Figure S4B), we observed no temperature-evoked responses in ASE neurons expressing any individual chimeric protein (Figure S4C). Similarly, GCY-8::GCY-1 chimeras trafficked correctly to the AFD sensory endings (Figure S4B), but unlike full-length GCY-8 protein, failed to restore temperature responses in AFD neurons of animals triply mutant for all three AFD-rGCs (Figure S4D). These results indicate that the inability of AFD-rGC::GCY-1 chimeras to mediate temperature responses is not restricted to a specific cellular context.

We next asked whether similar chimeras between GCY-23 and GCY-18 would be sufficient to confer temperature responses upon ectopic expression. Indeed, we found that expression of all examined GCY-23::GCY-18 chimeras (Figure 4D) resulted in robust temperature responses in ASER (Figure 4E), suggesting that both the extracellular and intracellular domains (ECD and ICD) of AFD-rGCs may be required for to confer thermosensory responses. Intriguingly, we noted that while T^*_{ASE} in neurons misexpressing any GCY-23::GCY-18 chimeric construct was higher than that in neurons expressing GCY-23 alone, neurons expressing chimeric proteins containing the GCY-18

ICD and transmembrane domain (TMD) exhibited a higher *T** than those expressing proteins containing the corresponding GCY-23 domains (Table S1). Together, these observations suggest that both the ECD and ICD of AFD-rGCs may be necessary for these proteins to mediate thermosensation, and that the ICD contributes to setting the *T**.

GCY-8 can mediate thermoresponses in AFD in the absence of either GCY-18 or GCY-23 (Inada et al., 2006) (Figure 1A, Figure S4D), but is unable to confer temperature responses upon misexpression (Figure 3A-B, Figure 4A), raising the possibility that GCY-8 is activated via AFD-specific mechanisms. To further address this issue, we examined the ability of GCY-8::GCY-18 and GCY-8::GCY-23 chimeras (Figure 4D) to confer temperature responses upon ectopic expression in ASE. Chimeras containing the GCY-8$^{(ECD)}$ but not the GCY-8$^{(ICD)}$ conferred temperature responses in ASER under the examined conditions, although responses were observed in only a subset of GCY-8$^{(ECD+TM)}$::GCY-23$^{(ICD)}$ –expressing neurons (Figure 4F). These results suggest that factors present in AFD or chemosensory neurons may activate or inhibit GCY-8 function, respectively, via interaction with the GCY-8$^{(ICD)}$.

DISCUSSION

We have shown that AFD-rGCs are necessary in AFD, and sufficient when expressed in multiple non-thermosensory cell types, to confer highly sensitive temperature responses. Each AFD-rGC confers responses in a distinct temperature range in different cell types. Previous work indicated that T^*_{AFD} is regulated by intracellular cGMP and calcium concentrations and appears to be a cell-intrinsic property (Ramot et al., 2008; Wang et al., 2013; Wasserman et al., 2011; Yu et al., 2014). We suggest that

the distinct activation temperatures of AFD-rGCs is a consequence of the resting levels of intracellular cGMP and calcium in misexpressing cells and tissues. As in mammalian photoreceptors, intracellular calcium levels may be read out by calcium sensor proteins such as guanylyl cyclase activating proteins (GCAPs) (Lim et al., 2014; Sharma and Duda, 2012) to modulate rGC enzymatic activity in a cell type-specific manner. Indeed, loss of function of the NCS-1 neuronal calcium sensor results in a higher T^*_{AFD} (Wang et al., 2013) and altered thermotaxis behaviors (Gomez et al., 2001). T^*_{AFD} is also highly flexible and is regulated by T_c experience via both transcription-dependent and –independent mechanisms (Yu et al., 2014). The absence of these mechanisms in misexpressing cells may partly underlie the weak T_c-dependent modulation of T^* upon ectopic expression. We conclude that AFD-rGCs are instructive for thermosensation, but that the activation temperature of individual AFD-rGCs is cell context-dependent. We and others have been unable to confer AFD-rGC-mediated temperature responses onto heterologous cells, in part due to defects in membrane trafficking of these proteins (D. Glauser and M. Goodman, personal communication; G. Budelli, Y.V.Y., A.T. and P.S., unpublished), thus it remains possible that additional factors contribute to their thermosensory functions.

Analysis of the thermosensory responses conferred by chimeric proteins suggests that both the ECD and ICD of AFD-rGCs contribute to their thermoresponsive properties. The presence of the GCY-18 or GCY-23 ICD and TMD in chimeric protein combinations generally correspond to a higher or lower T^*, respectively, suggesting that the T^* may in part be regulated via these domains, possibly via interaction with proteins such as GCAPs (Duda et al., 1996; Laura et al., 1996). The absence of such activation mechanisms, or the

presence of inhibitory factors, may account for the inability of GCY-8, or chimeras containing the GCY-8$^{(ICD)}$, to confer temperature responses upon misexpression. However, the ECDs of thermosensory rGCs are also necessary for temperature responses. Conformational changes upon ligand binding have been reported in transmembrane cyclases, resulting in allosteric activation of their enzymatic functions (Misono et al., 2005; Ogawa et al., 2004). Temperature responses by AFD-rGCs may require similar temperature-regulated conformational changes. Further analyses of thermosensory responses conferred by chimeric rGCs may allow us to identify residues in these proteins that contribute to thermosensation, and T^* plasticity.

In addition to temperature-dependent regulation of rGC enzymatic activity, additional mechanisms contribute to the extraordinary thermosensitivity of AFD (Ramot et al., 2008). Similar to observations in mammalian photoreceptors, these mechanisms include the high density and compartmentalization of thermosensory molecules in the membranes of the complex AFD microvilli (Nguyen et al., 2014), as well as T_c-dependent adaptation of T^*_{AFD} that decreases gain and increases thermosensitivity (Biron et al., 2006; Ramot et al., 2008; Yu et al., 2014). The expression of highly thermosensitive AFD-rGCs together with neuron-specific amplification and adaptation mechanisms allows AFD, and hence *C. elegans*, to be exquisitely temperature sensitive across a wide temperature range. A thermosensory signaling cascade has also been proposed to amplify thermoresponses in *Drosophila* (Kwon et al., 2008).

Intriguingly, recent work has shown that the guanylyl cyclase G rGC is both necessary and sufficient for sensing cool temperatures in the Grueneberg ganglion in the mouse nose (Chao et al., 2015). Identification of rGCs as possible thermosensitive

proteins in rodents and *C. elegans* further diversifies the functions of these versatile signaling proteins, and implies that thermosensory roles of these molecules may be conserved across phyla.

Experimental Procedures

Detailed protocols are provided in Supplemental Experimental Procedures.

Author Contributions

Conceptualization, A.T., Y.V.Y, and P.S.; Methodology, A.T., Y.V.Y., T.O.; Validation, A.T., Y.V.Y., V.M.H., H.W.B.; Investigation, A.T., Y.V.Y., V.M.H., H.W.B.; Writing and Editing, A.T., Y.V.Y., V.M.H., and P.S.; Supervision and Funding Acquisition, P.S.

Acknowledgments

We are grateful to K. Watkins, F. Pontiggia, G. Budelli and M. O'Donnell for assistance with experiments and data analyses, and the *Caenorhabditis* Genetics Center, K. Shen, W. Schafer, and Y. Zhang for reagents. We thank M. Goodman and E. Marder for discussions, and the Sengupta lab, M. Goodman, C. Bargmann, and P. Garrity for comments on the manuscript. This work was funded in part by the NIH (R01 GM081639 and P01 GM103770 – P.S., T32007292 – V.M.H. and P01NS079419 - T.O.).

FIGURE LEGENDS

Figure 1. AFD-specific rGCs are necessary for thermotransduction and thermosensory plasticity in AFD.

A) Average temperature-evoked ratiometric fluorescence changes in AFD neurons expressing cameleon YC3.6 in animals of the indicated genotypes. Errors are SEM. n=10 neurons each. T_c=20°C. The rate, frequency, and amplitude of temperature change (black line at top) was 0.02°C/sec, 0.04 Hz, and 0.5°C, respectively. Also see Figure S1.

B) Average T^*_{AFD} exhibited by animals of the indicated genotypes grown at T_c=20°C. T^*_{AFD} values were calculated from traces shown in A. *** indicate different from wild-type at P<0.001 (ANOVA and Bonferroni posthoc corrections for multiple comparisons).

Figure 2. AFD-rGCs confer thermosensitivity upon ectopic expression in chemosensory neurons.

A-B) Average fluorescence changes in ASEL, ASER and AWB neurons expressing GCaMP3 in the indicated genetic backgrounds, and/or upon ectopic expression of *gcy-8*, *gcy-18* and *gcy-23* to the shown rising temperature stimuli (black lines at top, 0.02°C/sec). Alleles used were *tax-4(p678)*, *gcy-8(oy44)*, *gcy-18(nj38)* and *gcy-23(nj37)*. Errors are SEM. n = 9-10 neurons each. Responses are pooled and averaged from two independent transgenic lines for each case. Also see Table S1.

C) GCaMP3 fluorescence changes in AFD (top), AWB (middle) and AWB neurons misexpressing GCY-8, GCY-18 and GCY-23 (bottom) in response to temperature transients. Traces at left show mean temperature transients and normalized fluorescence changes (ΔF/F) for three nominal temperature transients (ΔT = 0.4°C - blue, 0.8°C - red,

1.2°C - yellow) from a holding temperature (T_{hold}: AFD = 19.0°C, AWB = 22.1°C). Errors are SD. n=10 neurons each. T_c=20°C. Scatter plots at right show log mean peak fluorescence amplitudes for each temperature transient. Responses from individual animals are color coded. Lines are linear regression fits for each animal. The effective Q_{10} is shown ±95% confidence intervals, computed for each condition by fitting a mixed-effects linear model.

D) Average turn numbers (±SEM) exhibited by wild-type (solid bars) or transgenic (hatched bars) animals expressing all three AFD-rGCs in AWB under the *str-1* promoter. Non-GCaMP-expressing siblings of transgenic animals used in **A** and **B** above were examined. Animals were either maintained at 15°C (left) or subjected to a 15°C-28°C rising ramp (right). Turns are binned into 5 min intervals. Monitored temperature on the plate surface at the indicated times are shown. ** and *** - different from corresponding wild-type at P<0.01 and 0.001 (t-test), respectively. n=10 experiments of 15 animals each.

Figure 3. GCY-23 confers responses in the physiological temperature range upon ectopic expression in neurons and muscles.

A-B) Average fluorescence changes in AWB and ASER neurons expressing GCaMP3 and/or the indicated genes to the shown rising temperature stimuli (black lines at top, 0.02°C/sec). Errors are SEM. n = 7-10 neurons each. Responses are pooled and averaged from two independent transgenic lines each. Control data in **A-B** are repeated from Figure 2A-B for comparison and are indicated by dashed lines. Also see Figure S2 and Table S1.

C) Representative images showing localization of GFP-tagged AFD-rGC proteins at the distal dendritic ends of AWB (arrows). Anterior is at left. Scale bar: 10 μm.

D) Scatter plot showing GCaMP3 fluorescence changes in vulval muscles in individual animals expressing GCaMP3 and/or the indicated genes to a rising temperature stimulus (0.02°C/sec). Area under the curve (AUC) was calculated from the first 60 sec of the response following the first response above threshold. See Figure S3 for calcium responses of individual animals. rGC and *tax-2/4* cDNAs were expressed under the *unc-103e* or *myo-3* promoters, respectively. Horizontal black bars indicate the median. n = 8-10 neurons each. Responses are pooled and averaged from at least two independent transgenic lines each.

Figure 4. GCY-18 confers responses in noxious temperature ranges upon ectopic expression in chemosensory neurons.

A-C) Average fluorescence changes in AWB and ASER neurons expressing GCaMP3 and/or the indicated genes to the shown rising temperature stimuli (black lines, 0.02°C/sec) in the shown genetic backgrounds. The *tax-4(p678)* allele was examined in **B**. *gcy* cDNAs were expressed under the *str-1* (AWB) or *flp-6* (ASE) promoters. Errors are SEM. n = 7-10 neurons each. All shown responses are averaged from two independent transgenic lines each. Also see Figure S2 and Table S1.

D) Cartoon representation of the domain organization of rGCs and rGC chimeric proteins examined in **E** and **F**. Ovals, rectangles, diamonds and Pac-man shapes represent the extracellular domain (ECD), transmembrane domain (TMD), kinase homology domain, and guanylyl cyclase domain, respectively. Also see Figure S4.

E-F) Temperature-evoked fluorescence changes in ASER neurons expressing GCaMP3 and the indicated rGC and rGC chimeric proteins under *gcy-5* or *flp-6* regulatory sequences. The rate of temperature change was 0.03°C/sec. Average fluorescence changes are shown in **E.** Errors are SEM. Responses are averaged from at least two independent transgenic lines. Average responses and responses of corresponding individual neurons from two transgenic lines each are shown with thick and thin lines in the same color in **F**. n = 7-16 neurons each. Also see Figure S4 and Table S1.

REFERENCES

Barbagallo, B., and Garrity, P.A. (2015). Temperature sensation in *Drosophila*. Curr. Opin. Neurobiol. *34C*, 8-13.

Bargmann, C.I. (2006). Chemosensation in *C. elegans*. In Wormbook: A review of *C. elegans* biology, M. Chalfie, ed., pp. 1-29.

Bernstein, J.G., Garrity, P.A., and Boyden, E.S. (2012). Optogenetics and thermogenetics: technologies for controlling the activity of targeted cells within intact neural circuits. Curr. Opin. Neurobiol. *22*, 61-71.

Biron, D., Shibuya, M., Gabel, C., Wasserman, S.M., Clark, D.A., Brown, A., Sengupta, P., and Samuel, A.D. (2006). A diacylglycerol kinase modulates long-term thermotactic behavioral plasticity in *C. elegans*. Nat. Neurosci. *9*, 1499-1505.

Chao, Y.C., Chen, C.C., Lin, Y.C., Breer, H., Fleischer, J., and Yang, R.B. (2015). Receptor guanylyl cyclase-G is a novel thermosensory protein activated by cool temperatures. EMBO J *34*, 294-306.

Clark, D.A., Biron, D., Sengupta, P., and Samuel, A.D.T. (2006). The AFD sensory neurons encode multiple functions underlying thermotactic behavior in *C. elegans*. J. Neurosci. *26*, 7444-7451.

Duda, T., Goraczniak, R., Surgucheva, I., Rudnicka-Nawrot, M., Gorczyca, W.A., Palczewski, K., Sitaramayya, A., Baehr, W., and Sharma, R.K. (1996). Calcium modulation of bovine photoreceptor guanylate cyclase. Biochemistry *35*, 8478-8482.

Garrity, P.A., Goodman, M.B., Samuel, A.D., and Sengupta, P. (2010). Running hot and cold: behavioral strategies, neural circuits, and the molecular machinery for thermotaxis in *C. elegans* and *Drosophila*. Genes Dev. *24*, 2365-2382.

Gomez, M., De Castro, E., Guarin, E., Sasakura, H., Kuhara, A., Mori, I., Bartfai, T., Bargmann, C.I., and Nef, P. (2001). Ca^{2+} signaling via the neuronal calcium sensor-1 regulates associative learning and memory in *C. elegans*. Neuron *30*, 241-248.

Gray, J.M., Hill, J.J., and Bargmann, C.I. (2005). A circuit for navigation in *Caenorhabditis elegans*. Proc. Natl. Acad. Sci. USA *102*, 3184-3191.

Ha, H.I., Hendricks, M., Shen, Y., Gabel, C.V., Fang-Yen, C., Qin, Y., Colon-Ramos, D., Shen, K., Samuel, A.D., and Zhang, Y. (2010). Functional organization of a neural network for aversive olfactory learning in *Caenorhabditis elegans*. Neuron *68*, 1173-1186.

Hedgecock, E.M., and Russell, R.L. (1975). Normal and mutant thermotaxis in the nematode *Caenorhabditis elegans*. Proc. Natl. Acad. Sci. USA *72*, 4061-4065.

Hills, T., Brockie, P.J., and Maricq, A.V. (2004). Dopamine and glutamate control area-restricted search behavior in *Caenorhabditis elegans*. J. Neurosci. *24*, 1217-1225.

Hobert, O. (2013). The neuronal genome of *Caenorhabditis elegans*. WormBook, 1-106.

Inada, H., Ito, H., Satterlee, J., Sengupta, P., Matsumoto, K., and Mori, I. (2006). Identification of guanylyl cyclases that function in thermosensory neurons of *Caenorhabditis elegans*. Genetics *172*, 2239-2252.

Kimura, K.D., Miyawaki, A., Matsumoto, K., and Mori, I. (2004). The *C. elegans* thermosensory neuron AFD responds to warming. Curr. Biol. *14*, 1291-1295.

Kobayashi, K., Nakano, S., Amano, M., Tsuboi, D., Nishioka, T., Ikeda, S., Yokoyama, G., Kaibuchi, K., and Mori, I. (2016). Single-cell memory regulates a neural circuit for sensory behavior. Cell Rep. *14*, 11-21.

Kwon, Y., Shim, H.S., Wang, X., and Montell, C. (2008). Control of thermotactic behavior via coupling of a TRP channel to a phospholipase C signaling cascade. Nat. Neurosci. *11*, 871-873.

Laura, R.P., Dizhoor, A.M., and Hurley, J.B. (1996). The membrane guanylyl cyclase, retinal guanylyl cyclase-1, is activated through its intracellular domain. J. Biol. Chem. *271*, 11646-11651.

Lim, S., Dizhoor, A.M., and Ames, J.B. (2014). Structural diversity of neuronal calcium sensor proteins and insights for activation of retinal guanylyl cyclase by GCAP1. Front. Mol. Neurosci. *7*, 19.

Liu, S., Schulze, E., and Baumeister, R. (2012). Temperature- and touch-sensitive neurons couple CNG and TRPV channel activities to control heat avoidance in *Caenorhabditis elegans*. PLoS One *7*, e32360.

Liu, Y., Ruoho, A.E., Rao, V.D., and Hurley, J.H. (1997). Catalytic mechanism of the adenylyl and guanylyl cyclases: modeling and mutational analysis. Proc. Natl. Acad. Sci. USA *94*, 13414-13419.

Misono, K.S., Ogawa, H., Qiu, Y., and Ogata, C.M. (2005). Structural studies of the natriuretic peptide receptor: a novel hormone-induced rotation mechanism for transmembrane signal transduction. Peptides *26*, 957-968.

Mori, I., and Ohshima, Y. (1995). Neural regulation of thermotaxis in *Caenorhabditis elegans*. Nature *376*, 344-348.

Morton, D.B. (2004). Invertebrates yield a plethora of atypical guanylyl cyclases. Mol. Neurobiol. *29*, 97-116.

Nguyen, P.A., Liou, W., Hall, D.H., and Leroux, M.R. (2014). Ciliopathy proteins establish a bipartite signaling compartment in a *C. elegans* thermosensory neuron. J. Cell Sci. *127*, 5317-5330.

Ogawa, H., Qiu, Y., Ogata, C.M., and Misono, K.S. (2004). Crystal structure of hormone-bound atrial natriuretic peptide receptor extracellular domain: rotation mechanism for transmembrane signal transduction. J. Biol. Chem. *279*, 28625-28631.

Ortiz, C.O., Etchberger, J.F., Posy, S.L., Frokjaer-Jensen, C., Lockery, S., Honig, B., and Hobert, O. (2006). Searching for neuronal left/right asymmetry: genomewide analysis of nematode receptor-type guanylyl cyclases. Genetics *173*, 131-149.

Ortiz, C.O., Faumont, S., Takayama, J., Ahmed, H.K., Goldsmith, A.D., Pocock, R., McCormick, K.E., Kunimoto, H., Iino, Y., Lockery, S., *et al.* (2009). Lateralized gustatory behavior of *C. elegans* is controlled by specific receptor-type guanylyl cyclases. Curr. Biol. *19*, 996-1004.

Ramot, D., MacInnis, B.L., and Goodman, M.B. (2008). Bidirectional temperature-sensing by a single thermosensory neuron in *C. elegans*. Nat. Neurosci. *11*, 908-915.

Sharma, R.K., and Duda, T. (2012). Ca(2+)-sensors and ROS-GC: interlocked sensory transduction elements: a review. Front. Mol. Neurosci. *5*, 42.

Smith, H.K., Luo, L., O'Halloran, D., Guo, D., Huang, X.Y., Samuel, A.D., and Hobert, O. (2013). Defining specificity determinants of cGMP mediated gustatory sensory transduction in *Caenorhabditis elegans*. Genetics *194*, 885-901.

Tang, W.J., Stanzel, M., and Gilman, A.G. (1995). Truncation and alanine-scanning mutants of type I adenylyl cyclase. Biochemistry *34*, 14563-14572.

Terrien, J., Perret, M., and Aujard, F. (2011). Behavioral thermoregulation in mammals: a review. Front. Biosci. (Landmark Ed) *16*, 1428-1444.

Thompson, D.K., and Garbers, D.L. (1995). Dominant negative mutations of the guanylyl cyclase-A receptor. Extracellular domain deletion and catalytic domain point mutations. J. Biol. Chem. *270*, 425-430.

Tsalik, E.L., and Hobert, O. (2003). Functional mapping of neurons that control locomotory behavior in *Caenorhabditis elegans*. J. Neurobiol. *56*, 178-197.

Vriens, J., Nilius, B., and Voets, T. (2014). Peripheral thermosensation in mammals. Nat. Rev. Neurosci. *15*, 573-589.

Wang, D., O'Halloran, D., and Goodman, M.B. (2013). GCY-8, PDE-2, and NCS-1 are critical elements of the cGMP-dependent thermotransduction cascade in the AFD neurons responsible for *C. elegans* thermotaxis. J. Gen. Physiol. *142*, 437-449.

Wasserman, S.M., Beverly, M., Bell, H.W., and Sengupta, P. (2011). Regulation of response properties and operating range of the AFD thermosensory neurons by cGMP signaling. Curr. Biol. *21*, 353-362.

Yoshida, A., Nakano, S., Suzuki, T., Ihara, K., Higashiyama, T., and Mori, I. (2015). A glial K /Cl cotransporter modifies temperature-evoked dynamics in *C. elegans* sensory neurons. Genes Brain Behav. gbb:12260.

Yu, Y.V., Bell, H.W., Glauser, D.A., Goodman, M.B., Van Hooser, S.D., and Sengupta, P. (2014). CaMKI-dependent regulation of sensory gene expression mediates experience-dependent plasticity in the operating range of a thermosensory neuron. Neuron *84*, 919-926.

Figure 1

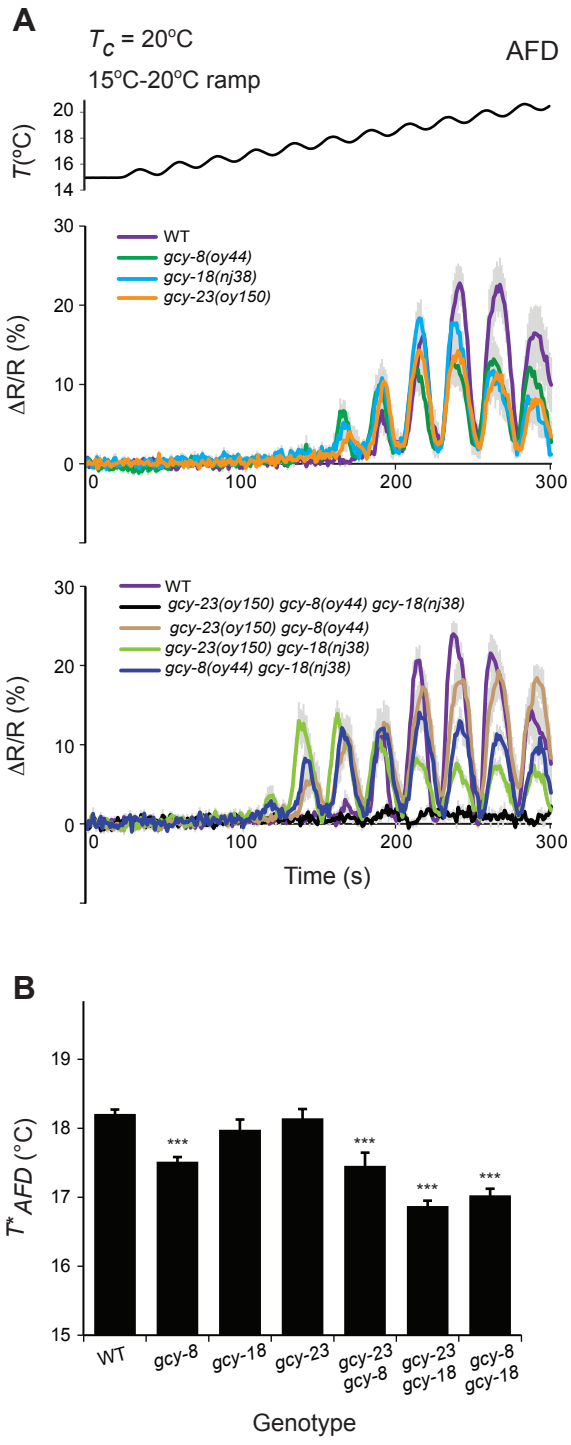
A
T_c = 20°C
15°C-20°C ramp
AFD
T(°C)
20
18
16
14
ΔR/R (%)
30
20
10
0
0
100
200
300
WT
gcy-8(oy44)
gcy-18(nj38)
gcy-23(oy150)
WT
gcy-23(oy150) gcy-8(oy44) gcy-18(nj38)
gcy-23(oy150) gcy-8(oy44)
gcy-23(oy150) gcy-18(nj38)
gcy-8(oy44) gcy-18(nj38)
Time (s)
B
T* AFD (°C)
19
18
17
16
15
***
WT
gcy-8
gcy-18
gcy-23
gcy-23 gcy-8
gcy-23 gcy-18
gcy-8 gcy-18
Genotype

Figure 2

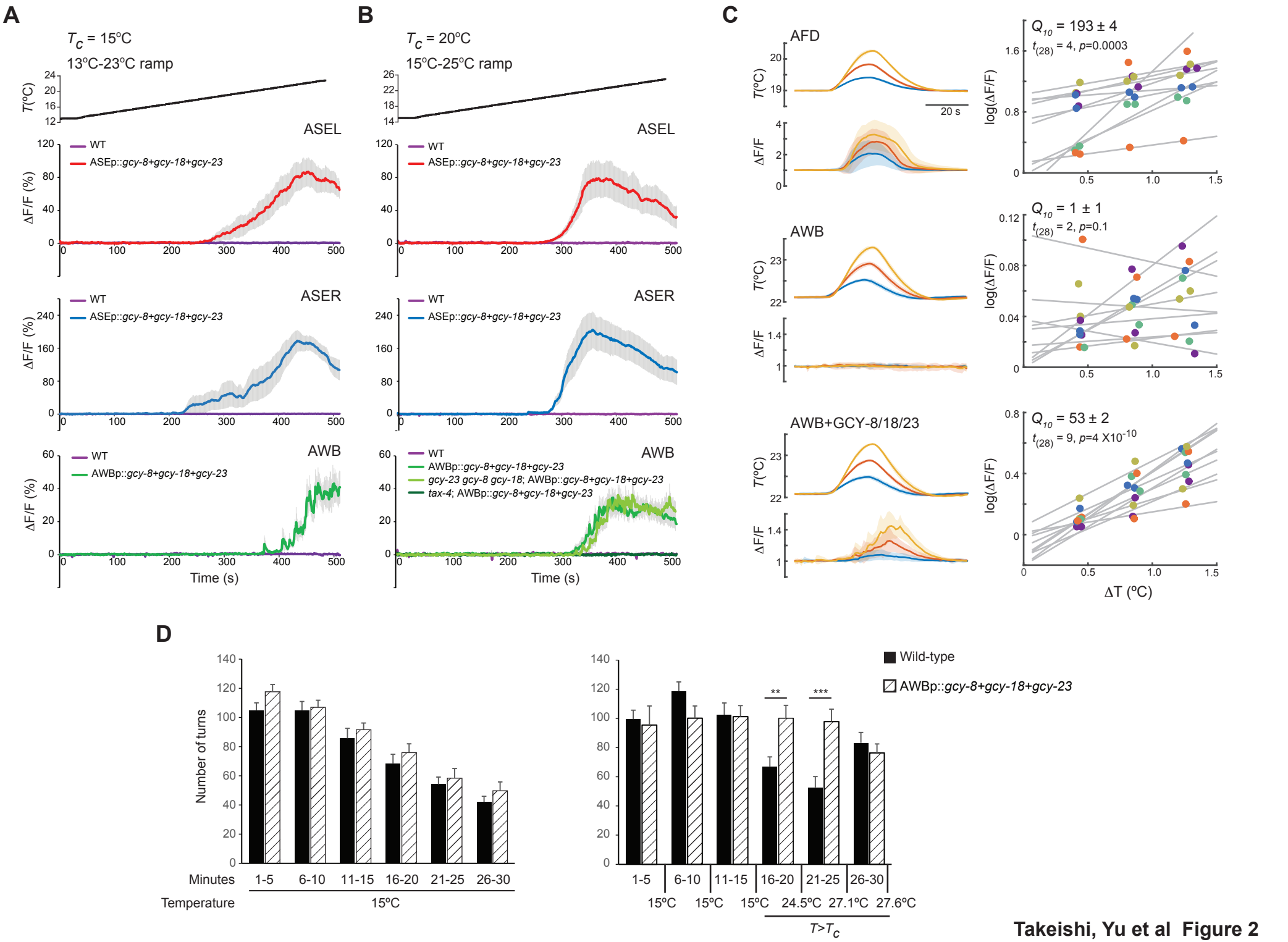

Takeishi, Yu et al Figure 2

Figure 3

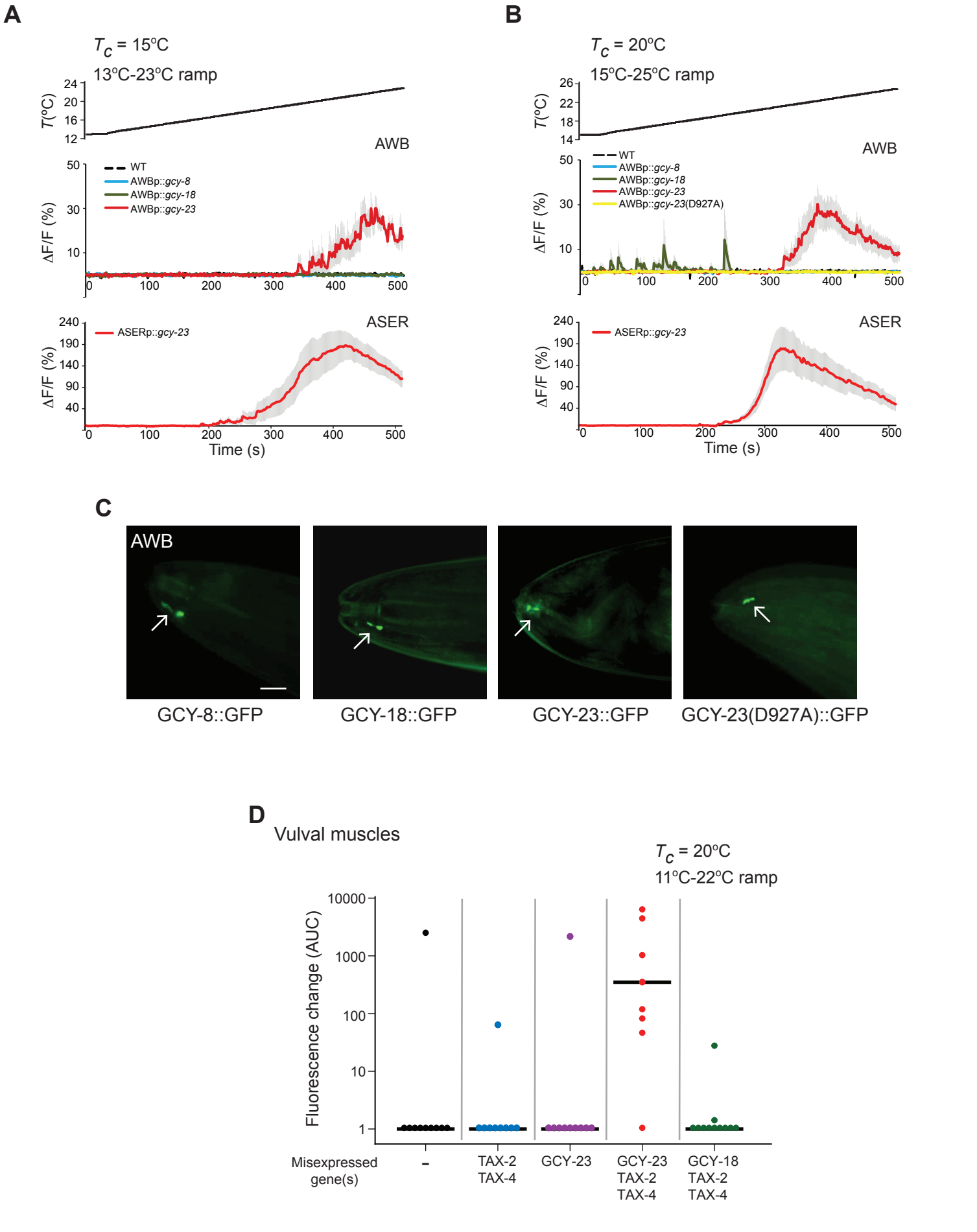

Takeishi, Yu et al Figure 3

Figure 4

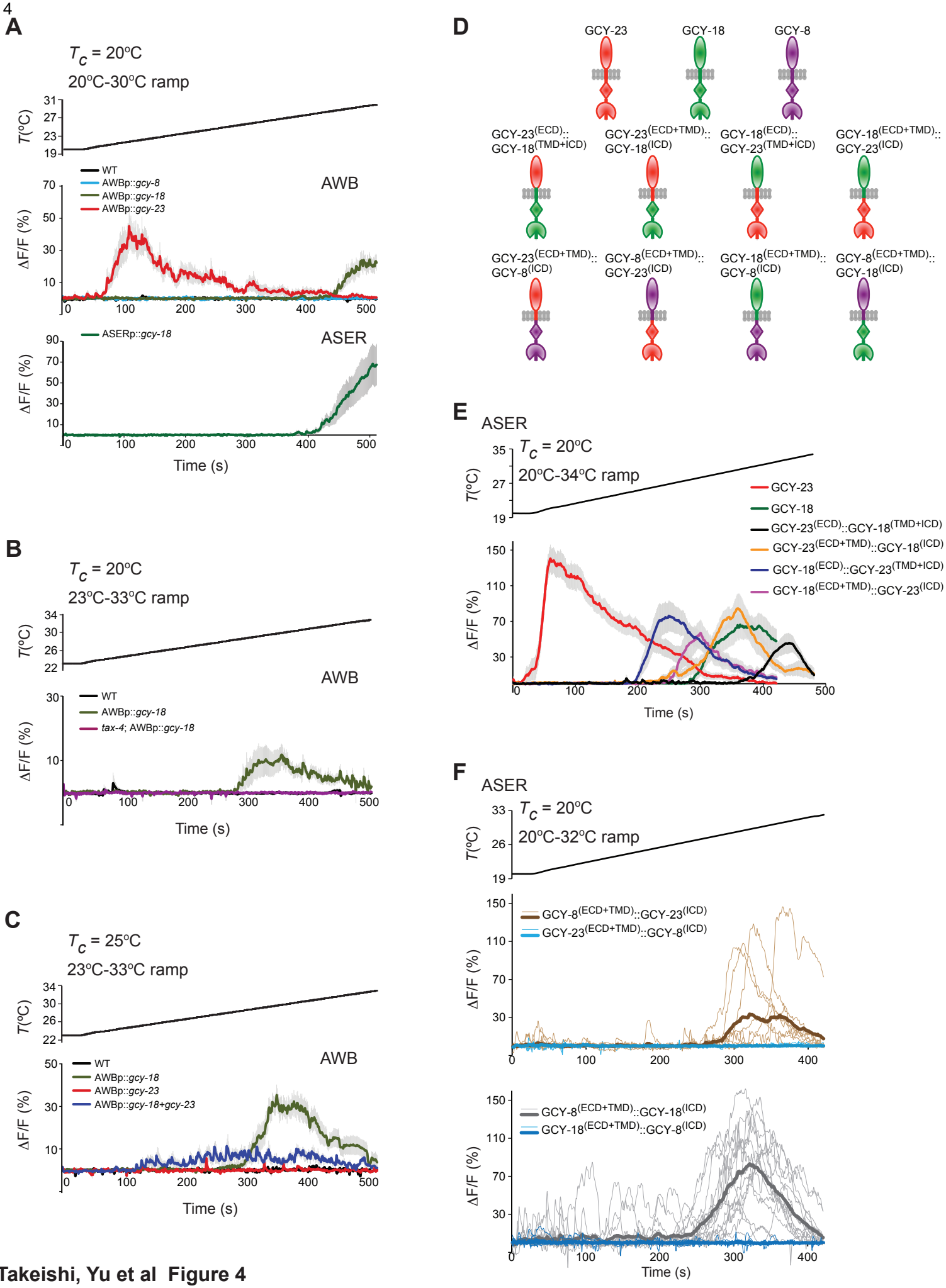

Takeishi, Yu et al Figure 4

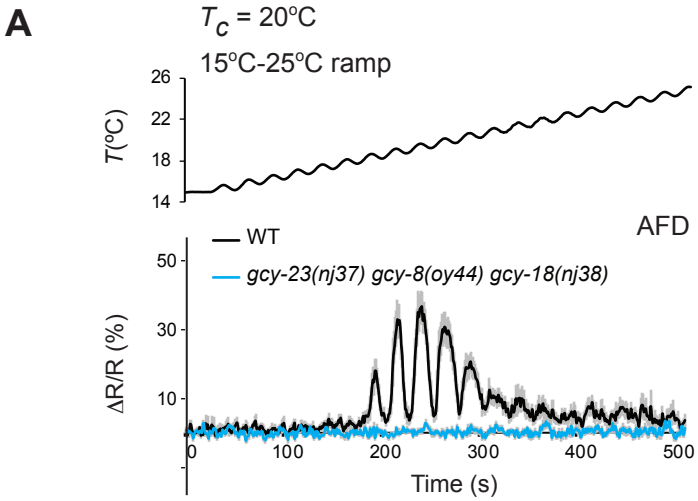

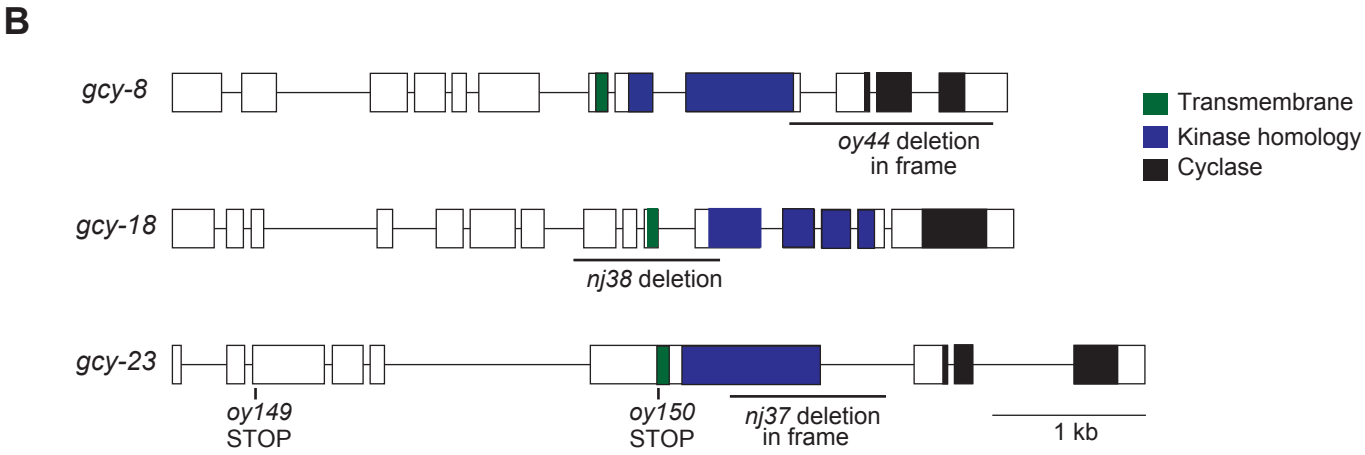

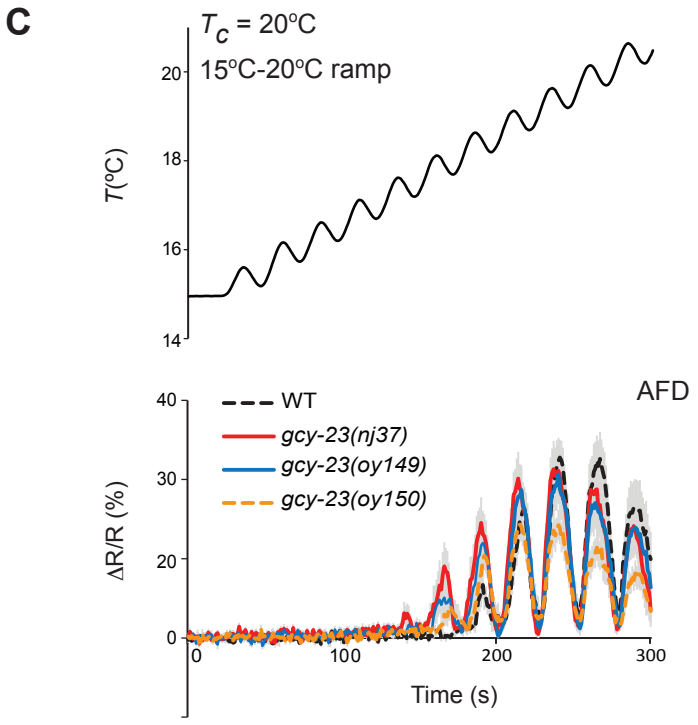

Takeishi, Yu et al, Figure S1 related to Figure 1

Figure S1 related to Figure 1. AFD-rGCs are necessary for thermotransduction in AFD.

A) Average ratiometric fluorescence changes in AFD neurons expressing YC3.6 in wild-type and *gcy-23(nj37) gcy-8(oy44) gcy-18(nj38)* mutants to the shown oscillating rising temperature ramp. The rate, frequency, and amplitude of temperature change was 0.02°C/sec, 0.04 Hz, and 0.5°C, respectively. Errors are SEM. n = 10 neurons each.

B) Predicted exon/intron structures of *gcy-8, gcy-18* and *gcy-23*. Filled boxes encode indicated domains. The locations and molecular nature of alleles used in this work are shown.

C) Average temperature-evoked ratiometric fluorescence changes in AFD neurons expressing cameleon YC3.6 in animals of the indicated genotypes. Errors are SEM. n=10 neurons each. T_c=20°C. The rate, frequency, and amplitude of temperature change was 0.02°C/sec, 0.04 Hz, and 0.5°C, respectively. Data for wild-type and *gcy-23(oy150)* animals are repeated from Figure 1 for comparison and are indicated by dashed lines.

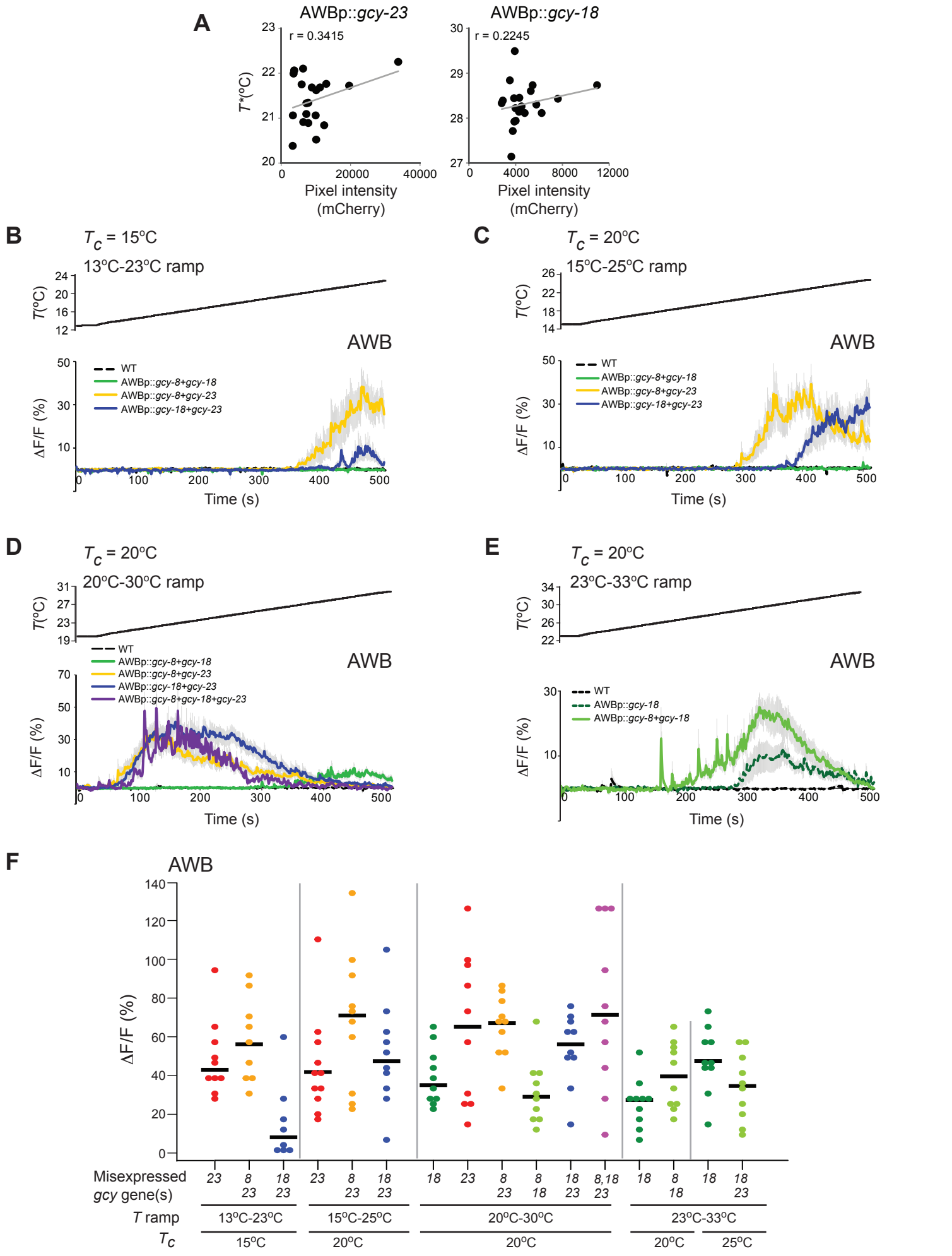

Takeishi, Yu et al Figure S2 related to Figures 3 and 4

Figure S2 related to Figures 3 and 4. Temperature responses conferred upon expression of AFD-rGCs in chemosensory neurons.

A) Correlation between mCherry fluorescence levels and T^* in individual AWB neurons (filled circles) expressing *rGC::SL2::mCherry*. *r* indicates the Pearson correlation coefficient. T_c=20°C; n=20 neurons each.

B-E) Average fluorescence changes in AWB neurons expressing GCaMP3 and/or the indicated genes to the shown rising temperature stimuli (black lines, 0.02°C/sec). *gcy* cDNAs were expressed under the *str-1* promoter in AWB, and coinjected at the same concentration each. Errors are SEM. n = 7-10 neurons each. All shown responses are averaged from two independent transgenic lines each. Peak response amplitudes of individual neurons are shown in **F**. Control data in **B-E** and *gcy-18* data in **E** are repeated from Figures 2 and 4 for comparison and are indicated by dashed lines.

F) Scatter plot of peak response amplitudes of individual neurons whose averaged responses are shown in Figures 3A-B, 4A-C and S2B-E. Horizontal black bars indicate medians. Response amplitudes are shown only for those strains in which responses above threshold (see Supplemental Experimental Procedures) were observed in one or more examined neurons.

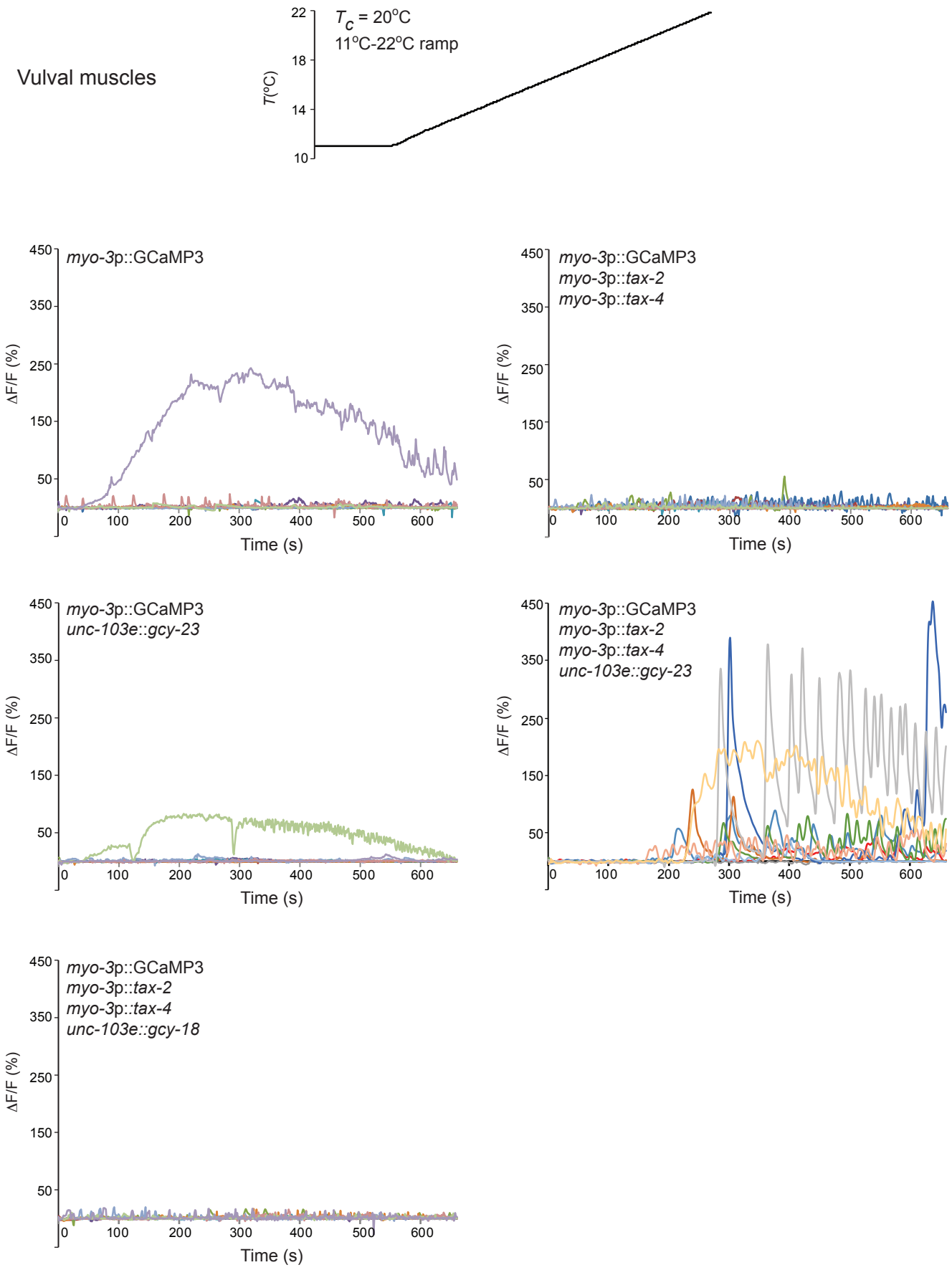

Takeishi, Yu et al, Figure S3 related to Figure 3

Figure S3 related to Figure 3. GCY-23 confers temperature responses upon ectopic expression in vulval muscles expressing TAX-2 and TAX-4.

Responses of individual animals expressing the indicated proteins in vulval muscles to the shown rising temperature stimulus (black line, 0.02°C/sec). Area under the curve during the first 60 seconds of the response are plotted in Figure 3D.

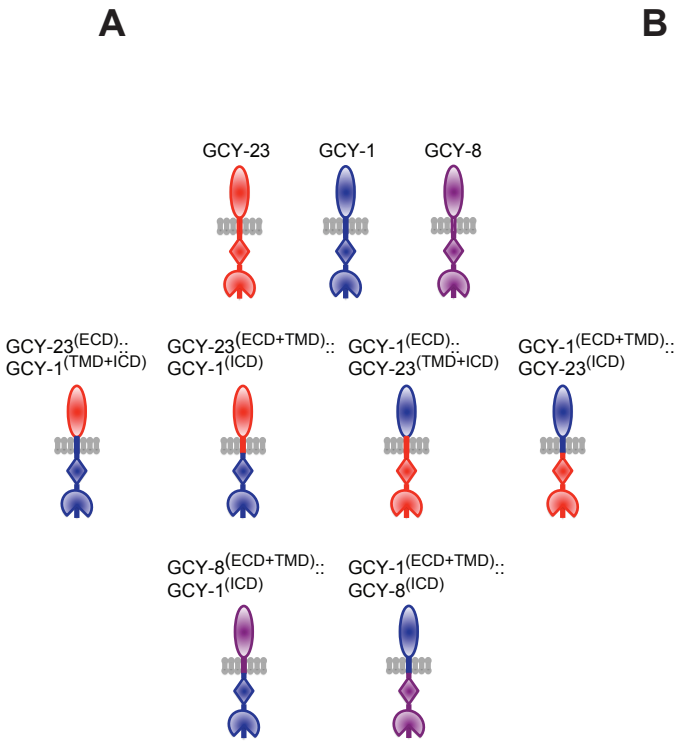

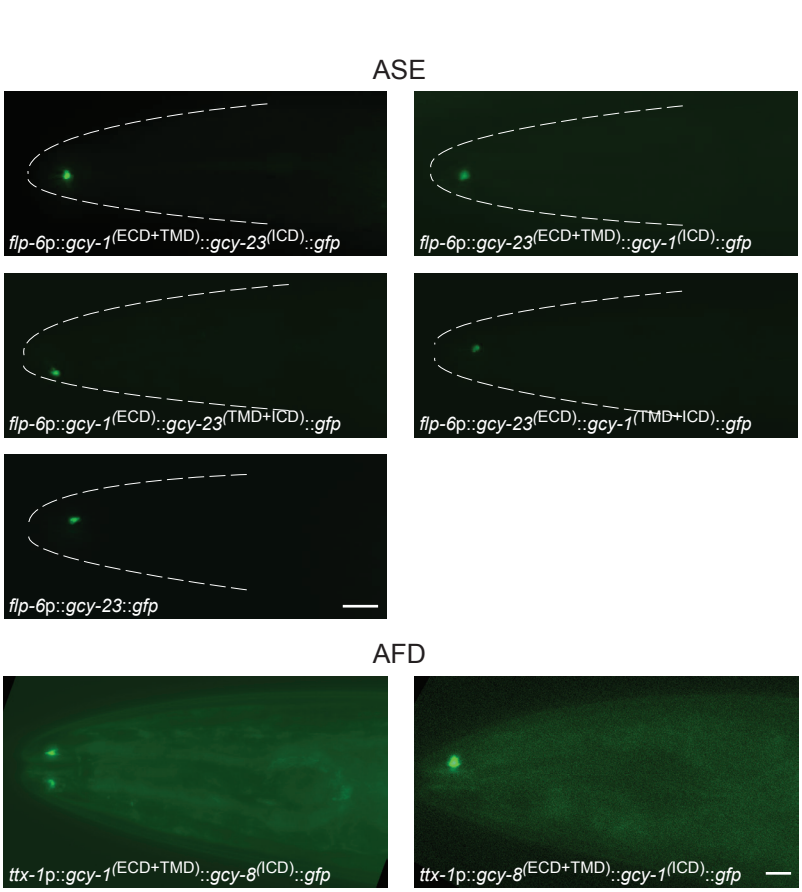

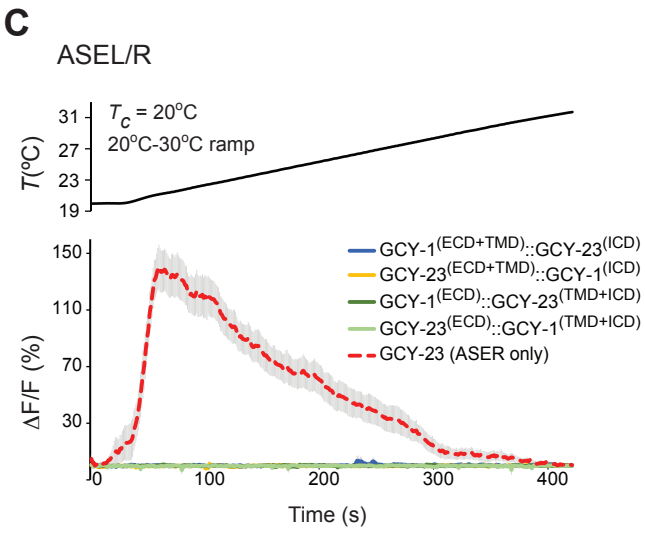

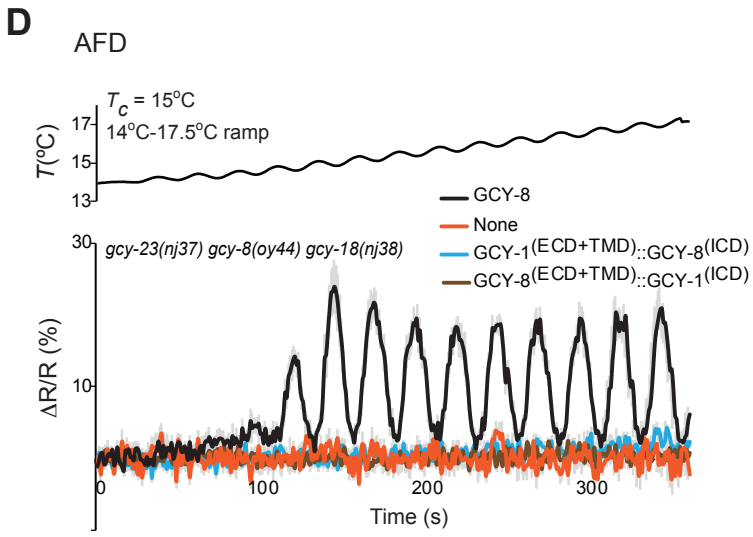

Takeishi, Yu et al Figure S4 related to Figure 4

Figure S4 related to Figure 4. Both the ICD and ECD domains may contribute to AFD-rGC thermosensory properties.

A) Cartoon representation of the domain organization of rGCs and rGC chimeric proteins as indicated in the legend to Figure 4D.

B) Localization of indicated chimeric proteins in ASE and AFD. Scale bars: 10 μm.

C) Average temperature-evoked fluorescence changes in ASEL/R neurons expressing GCaMP3 and the indicated rGC and rGC chimeric proteins. rGC and GCY-23::GCY-1 chimeric proteins were expressed under *flp-6* regulatory sequences. Errors are SEM. The rate of temperature change was 0.03°C/sec. All shown responses are averaged from at least two independent transgenic lines each. Responses of GCY-23 misexpressing neurons are repeated from Figure 4E for comparison purposes and are indicated by a dashed red line. n = 7-10 neurons each.

D) Average temperature-evoked ratiometric fluorescence changes in AFD neurons expressing cameleon YC3.6 in *gcy-23(nj37) gcy-8(oy44) gcy-18(nj38)* mutants expressing the indicated proteins under the *gcy-8* promoter. Errors are SEM. n=10 neurons each. T_c=15°C. The rate, frequency, and amplitude of temperature change was 0.01°C/sec, 0.04 Hz, and 0.2°C, respectively.

SUPPLEMENTAL MOVIE LEGENDS

Movie S1 related to Figure 2

Representative movie of temperature-evoked changes in GCaMP fluorescence in ASER neurons misexpressing *gcy-8*, *gcy-18* and *gcy-23*. T_c=20°C.

Movie S2 related to Figure 3

Representative movie of temperature-evoked changes in GCaMP fluorescence in AWB neurons misexpressing *gcy-23*. T_c=20°C.

Movie S3 related to Figure 3

Representative movie of temperature-evoked changes in GCaMP fluorescence in vulval muscles expressing *gcy-23*, *tax-2* and *tax-4*. T_c=20°C.

Table S1 related to Figures 1-4. The activation threshold (T^*) of AFD-rGCs is determined in a cell type-specific manner.

Misexpressed rGC[a] or *genotype*	Cell/Tissue	T_c (°C)	Temperature ramp (°C)	T^* (± SD)	*P*-value	T_{max} (± SD)[b]
WT	AFD	15	13-23	16.1 (0.5)		ND
WT	AFD	20	15-20	18.1 (0.3)	<0.001[c]	ND
GCY-8/18/23	ASEL	15	13-23	18.9 (0.8)		21.5 (0.4)
GCY-8/18/23	ASEL	20	15-25	20.5 (0.6)	<0.001[c]	22.1 (0.8)
GCY-8/18/23	ASER	15	13-23	19.1 (1.2)		21.5 (0.7)
GCY-8/18/23	ASER	20	15-25	20.4 (0.5)	0.007[c]	21.7 (0.5)
GCY-8/18/23	AWB	15	13-23	20.7 (0.6)		21.8 (0.6)
GCY-8/18/23	AWB	20	15-25	21.6 (0.5)	0.002[c]	22.7 (0.9)
GCY-8/18/23	AWB	20	20-30	21.4 (0.4)	0.006[c]	22.5 (1.0)
GCY-23	AWB	15	13-23	20.8 (0.8)		21.9 (0.7)
GCY-23	AWB	20	15-25	21.5 (0.4)	0.020[c]	22.4 (0.5)
GCY-23	ASER	15	13-23	18.5 (0.6)		20.8 (0.7)
GCY-23	ASER	20	15-25	20.0 (0.6)	<0.001[c]	21.5 (1.1)
GCY-23	AWB	20	20-30	21.0 (0.3)		22.4 (1.3)
GCY-18	AWB	20	20-30	28.6 (0.7)		29.5 (0.3)
GCY-18	ASER	20	20-30	28.2 (0.5)		29.8 (0.2)
GCY-18	AWB	15	23-33	28.8 (0.6)		29.7 (0.9)
GCY-18	AWB	20	23-33	29.6 (1.2)	0.077[c]	30.4 (1.1)
GCY-8/23	AWB	15	13-23	21.1 (0.8)	0.458[d]	22.0 (0.7)
GCY-8/23	AWB	20	15-25	21.4 (0.7)	0.769[d]	22.5 (0.7)
GCY-8/23	AWB	20	20-30	21.1 (0.4)	0.664[d]	21.9 (0.6)
GCY-8/18	AWB	20	20-30	27.1 (0.8)	<0.001[e]	28.2 (0.6)
GCY-8/18	AWB	20	23-33	27.0 (0.8)	<0.001[e]	28.2 (1.5)
GCY-18/23	AWB	15	13-23	20.9 (0.8)	0.875[d,f]	22.1 (0.4)[f]
GCY-18/23	AWB	20	15-25	22.9 (0.8)	<0.001[d]	24.1 (0.8)
GCY-18/23	AWB	20	20-30	21.2 (0.4)	0.326[d], <0.001[e]	22.7 (0.7)
GCY-18	AWB	25	23-33	28.8 (0.6)		29.5 (0.5)
GCY-18/23	AWB	25	23-33	26.3 (1.7)	<0.001[e]	28.8 (1.6)
GCY-23	VM	20	11-22	14.1 (1.0)		ND
gcy-8(oy44)	AFD	20	15-20	17.5 (0.2)	<0.001[g]	ND
gcy-18(nj38)	AFD	20	15-20	18.0 (0.4)	0.377[g]	ND
gcy-23(nj37)	AFD	20	15-20	17.9 (0.4)	0.377[g]	ND
gcy-23(oy149)	AFD	20	15-20	18.0 (0.4)	0.433[g]	ND
gcy-23(oy150)	AFD	20	15-20	18.1 (0.4)	0.991[g]	ND
gcy-23(oy150) gcy-8(oy44)	AFD	20	15-20	17.5 (0.6)	0.005[g]	ND
gcy-23(oy150) gcy-18(nj38)	AFD	20	15-20	16.9 (0.2)	<0.001[g]	ND
gcy-8(oy44) gcy-18(nj38)	AFD	20	15-20	17.0 (0.3)	<0.001[g]	ND
GCY-23	ASER	20	20-32	20.1 (0.0)		21.2 (0.2)
GCY-18	ASER	20	20-32	28.5 (0.3)		30.6 (0.8)
GCY-$23^{(ECD)}$::GCY-	ASER	20	20-32	31.0 (0.2)		32.6 (0.3)

$18^{(TMD+ICD)}$					
GCY-$23^{(ECD+TMD)}$::GCY-$18^{(ICD)}$	ASER	20	20-32	27.6 (0.3)	29.9 (1.0)
GCY-$18^{(ECD)}$::GCY-$23^{(TMD+ICD)}$	ASER	20	20-32	25.5 (0.3)	27.7 (1.4)
GCY-$18^{(ECD+TMD)}$::GCY-$23^{(ICD)}$	ASER	20	20-32	27.5 (0.4)	28.5 (0.8)

[a]rGCs were ectopically expressed under the following promoters: ASEL/R – *flp-6*; ASER- *gcy-5*; AWB – *str-1*; vulval muscles (VM) – *unc-103e*.
[b]T_{max} indicates the average temperature of peak response amplitude.
[c]As compared to values at 15°C in the same genetic background.
[d]As compared to values under the same conditions in neurons expressing GCY-23 alone.
[e]As compared to values under the same conditions in neurons expressing GCY-18 alone.
[f]Calculated from the subset of responding neurons (Figure S2F).
[g]As compared to values in wild-type animals under the same conditions.
n=7-10 neurons from at least two transgenic lines for each. ND – not done.

Table S2 related to all Figures. List of strains used in this work.

See Excel File.

SUPPLEMENTAL EXPERIMENTAL PROCEDURES

C. elegans strains

The wild-type strain was *C. elegans* variety Bristol, strain N2. Strains were maintained with *E. coli* OP50 as the food source. Transgenic animals were generated using test plasmids at 1-60 ng/µl and the *unc-122*p*::gfp, unc-122*p*::rfp* or *ttx-3*p*::gfp* coinjection markers at 30 or 50 ng/µl. Strains expressing genetically encoded calcium indicators were the following: PY9735 (*str-1*p::*GCaMP3*); ZC1600 (*flp-6*p::*GCaMP3*) (Luo et al., 2014)); PY8971 (*srtx-1*p::*YC3.6*) (Yu et al., 2014)); PY8339 (*gcy-8*p::*GCaMP3)*; AQ2364 (*myo-3*p::*GCaMP3*) (gift from W. Schafer) (Butler et al., 2015). The presence of specific mutations in a strain was confirmed by sequencing. A complete list of all strains used in this work is provided in Table S2.

Molecular biology

gcy cDNAs were amplified from a *C. elegans* cDNA library generated from a population of mixed stage animals, and verified via sequencing. To facilitate identification of transgenic animals misexpressing the rGCs in the appropriate cell type, rGC cDNAs were fused via a SL2 trans-splicing leader sequence to a *mCherry* reporter. *gcy* cDNAs were misexpressed under the following gene regulatory sequences: AWB – *str-1* (2.4 or 3.0 kb); ASEL/R – *flp-6* (2.7 kb), ASER - *gcy-5* (3.2 kb). The *gcy-23* and *gcy-18* cDNAs were expressed in vulval muscles under the *unc-103e* regulatory sequences (Reiner et al., 2006) (gift of K. Shen); *tax-2* and *tax-4* cDNAs were expressed under the *myo-3* promoter (2.5 kb). The sequence change encoding the D927A mutation in the *gcy-23* cDNA was introduced via PCR-based mutagenesis and confirmed by sequencing.

To generate GFP-tagged GCY proteins, sequences encoding GFP were introduced just prior to the STOP codon in the *gcy* cDNAs and the fusion genes were expressed under *srd-23, flp-6*, or *ttx-1* upstream regulatory sequences for expression in AWB, ASE, and AFD, respectively. Chimeric constructs between different *gcy* genes were generated using the Gibson assembly method (Gibson et al., 2009). Overlapping amplicons from different *gcy* genes were assembled with a linearized expression vector using the NEBuilder HiFi DNA assembly master mix. Constructs were verified via sequencing. Transmembrane domains of each GCY protein were predicted by the Simple Modular Architecture Tool (http://smart.embl-heidelberg.de/). The junction sites in each rGC are as follows (amino acid residues included in each domain are indicated in parentheses):

GCY-1: ECD(1-496), TMD(497-519), ICD(520-1137)

GCY-8: ECD(1-504), TMD(505-527), ICD(528-1152)

GCY-18: ECD(1-497), TMD(498-520), ICD(521-1113)

GCY-23: ECD(1-457), TMD(458-480), ICD(481-1073)

Chimeric constructs were expressed in ASE and AFD under *flp-6* or *gcy-5,* and *gcy-8,* regulatory sequences, respectively.

Generation of a *gcy-23* null allele via CRISPR/Cas9-mediated gene editing

The *gcy-23(oy149)* and *gcy-23(oy150)* alleles were generated via CRISPR/Cas9-mediated gene editing as described (Arribere et al., 2014; Paix et al., 2014; Zhao et al., 2014). In brief, *gcy-23* sgRNA sequences and *rol-6(su1006)* sgRNA sequences (Arribere et al., 2014; Friedland et al., 2013) were injected (at 25 ng/μl each) together with *gcy-23* and *rol-6(su1006)* oligonucleotides (at 500 nM each), and the Cas9-encoding plasmid

pDD162 (at 50 ng/µl) (Dickinson et al., 2013) into *gcy-8(oy44) gcy-18(nj38)* animals (Inada et al., 2006). F1 roller animals were isolated, and the presence of mutations in the *gcy-23* sequence was confirmed by amplification and sequencing. F2 non-roller progeny were further screened for the presence of the homozygous *gcy-23* mutation. Sequences of the *gcy-23* sgRNA and *gcy-23* donor oligonucleotides are provided below. Sequences of the *rol-6* sgRNA and *rol-6* oligonucleotides have been previously described (Arribere et al., 2014).

gcy-23(oy149) sgRNA: 5'- ATCCTGAACCAAATGGGATG – 3'

gcy-23(oy150) sgRNA: 5'- GCATCCTCCGATAATCAATG – 3'

gcy-23(oy149) oligonucleotide: 5' –
CTAGAACCTGTAATGTTTTCAGAATCCTGAACCAAATGGGTAAATAAATAAG
CAAAGAATCGTATGAAGGTGTTGCGGTAAGTGCAGACATGTACCATGTTCAA
GGAGTTCGTGCATTT -3'

gcy-23(oy150) oligonucleotide: 5' –
CAGAAGTACAATGCATCCTCCGATAATCATTATTTATTTATGTAATGTAGTCG
CATTTTTCATTTCGGAA -3''

***in vivo* calcium imaging**

Ca^{2+} imaging experiments were performed essentially as described previously (Yu et al., 2014). Imaging was performed in animals expressing the genetically encoded calcium indicators GCaMP3 in AWB, ASE, AFD, and muscle, or yellow cameleon YC3.6 in AFD (Clark et al., 2007; Wasserman et al., 2011; Yu et al., 2014). Misexpressing cells were identified via the expression of SL2::mCherry; animals

expressing similar levels of mCherry were selected for imaging to control for gene expression. To control for variability in expression of the calcium indicator (Hires et al., 2008), we only imaged animals expressing the indicator within an expression range defined experimentally for each cell type. Fluorescence intensities in the soma were quantified using ImageJ (NIH) software. Growth-synchronized L4 larval stage animals were cultivated overnight at specific temperatures, and young adults were imaged the next day for somal or vulval muscle calcium responses to temperature stimuli.

Individual animals were placed on a 10% agarose pad on a coverslip and immobilized with 1.5 μl of 2.5% (w/v) solution of 0.1 μm polystyrene beads (Polysciences), or freshly prepared 10 mM levamisole (Sigma Aldrich), and covered with a second glass coverslip. Sandwiched coverslips and animals were transferred and mounted with 5 μl of glycerol on a glass slide secured onto a Peltier on the microscope stage prewarmed to the desired starting temperature. Current delivery was controlled by temperature-regulated feedback using LabView (National Instruments) to achieve the desired target temperature; the temperature was measured using a 15K thermistor (McShane Inc). Animals were subjected to temperature ramps with 0.01°C/sec - 0.03°C/sec rates of temperature change as indicated in the figure legends. For imaging in AFD, a sinusoidal oscillation of 0.04 Hz and and 0.2°C-0.5°C amplitude was superimposed upon the linear temperature ramp to facilitate detection of T^*_{AFD} using the YC3.6 calcium indicator (Clark et al., 2006). Calcium dynamics in vulval muscles were initially assessed in response to different temperature stimuli in order to identify the responding range; all subsequent experiments were performed using the responding

temperature range. Baseline fluorescence was set to zero to offset fluorescence decreases caused by photobleaching or movement artifacts.

Images were captured using a Zeiss 40X air objective (NA 0.9) using MetaMorph software (Molecular Devices), and a digital camera (Orca, Hamamatsu) at a rate of 1 Hz. Data were analyzed using custom written scripts in MATLAB. T^* was defined as the temperature at which ΔF/F increased by a minimum of 2% over at least 8 consecutive seconds with an average slope of >0.3% per sec. In vulval muscles, T^* was defined as the temperature at which ΔF/F increased by >30%. For cells expressing YC3.6, T^* was defined as the temperature at which the YFP/CFP ratio first phase-locked to the sinusoidal variation in the stimulus. All shown responses are pooled and averaged from at least two independent transgenic lines each.

Q_{10} measurements

Since temperature-evoked calcium responses as detected by changes in GCaMP fluorescence saturate (Hires et al., 2008), we performed all measurements in a narrow temperature range around the corresponding T^* for each neuron. Q_{10} values were calculated from peak normalized fluorescence values ($\Delta F_{peak}/F$) obtained in response to five successive temperature transients (ΔT = 0.4°C, 0.8°C, 1.2°C, 0.8°C, 0.4°C) from a constant holding temperature (T_{hold}). Repeat measures at the lower and middle nominal temperature transients (ΔT = 0.4°C, 0.8°C) were averaged. The T_{hold} was selected as a temperature that was ~0.5°C higher than T^* for each neuron type under the examined conditions (T_c=20°C; AFD T_{hold} = 19.0°C; AWB T_{hold} = 22.1°C). We estimated Q_{10} using

the slope parameters of a mixed-effects linear model fitted to $\log(\Delta F_{peak}/F)$ with the unit of replication (animal, n=10 in all cases) as a random effect and ΔT as a fixed effect.

Behavior

Animals were cultivated overnight at 15ºC with food. Prior to the start of the assay, 15 young adult animals were transferred to a 10 cm unseeded NGM plate pre-chilled at 15ºC, which was in turn placed on an aluminum plate with the temperature set at 15ºC. The temperature on the aluminum plate was established and maintained by Peltier thermoelectric temperature controllers (Oven Industries). The temperature of the NGM plate was measured with a two probe digital thermometer (Fluke Electronics). Animals were assayed for locomotion on plates held at 15ºC for 15 min following which the temperature of the aluminum plate was raised to 28ºC or maintained at 15ºC for the remainder of the experiment. Animal movement was recorded at a rate of 1 Hz using a PixeLink CCD camera. Videos were analyzed using custom written scripts in MATLAB. A turn was defined as an instantaneous change in direction greater than 27.7ºC from the average run direction.

REFERENCES

Arribere, J.A., Bell, R.T., Fu, B.X., Artiles, K.L., Hartman, P.S., and Fire, A.Z. (2014). Efficient marker-free recovery of custom genetic modifications with CRISPR/Cas9 in *Caenorhabditis elegans*. Genetics *198*, 837-846.

Butler, V.J., Branicky, R., Yemini, E., Liewald, J.F., Gottschalk, A., Kerr, R.A., Chklovskii, D.B., and Schafer, W.R. (2015). A consistent muscle activation strategy underlies crawling and swimming in *Caenorhabditis elegans*. J. R. Soc. Interface *12*, 20140963.

Dickinson, D.J., Ward, J.D., Reiner, D.J., and Goldstein, B. (2013). Engineering the *Caenorhabditis elegans* genome using Cas9-triggered homologous recombination. Nat. Methods *10*, 1028-1034.

Friedland, A.E., Tzur, Y.B., Esvelt, K.M., Colaiacovo, M.P., Church, G.M., and Calarco, J.A. (2013). Heritable genome editing in *C. elegans* via a CRISPR-Cas9 system. Nat. Methods *10*, 741-743.

Gibson, D.G., Young, L., Chuang, R.Y., Venter, J.C., Hutchison, C.A., 3rd, and Smith, H.O. (2009). Enzymatic assembly of DNA molecules up to several hundred kilobases. Nat. Methods *6*, 343-345.

Hires, S.A., Tian, L., and Looger, L.L. (2008). Reporting neural activity with genetically encoded calcium indicators. Brain Cell Biol. *36*, 69-86.

Inada, H., Ito, H., Satterlee, J., Sengupta, P., Matsumoto, K., and Mori, I. (2006). Identification of guanylyl cyclases that function in thermosensory neurons of *Caenorhabditis elegans*. Genetics *172*, 2239-2252.

Luo, L., Wen, Q., Ren, J., Hendricks, M., Gershow, M., Qin, Y., Greenwood, J., Soucy, E.R., Klein, M., Smith-Parker, H.K.*, et al.* (2014). Dynamic encoding of perception, memory, and movement in a *C. elegans* chemotaxis circuit. Neuron *82*, 1115-1128.

Paix, A., Wang, Y., Smith, H.E., Lee, C.Y., Calidas, D., Lu, T., Smith, J., Schmidt, H., Krause, M.W., and Seydoux, G. (2014). Scalable and versatile genome editing using linear DNAs with microhomology to Cas9 Sites in *Caenorhabditis elegans*. Genetics *198*, 1347-1356.

Reiner, D.J., Weinshenker, D., Tian, H., Thomas, J.H., Nishiwaki, K., Miwa, J., Gruninger, T., Leboeuf, B., and Garcia, L.R. (2006). Behavioral genetics of *Caenorhabditis elegans unc-103*-encoded erg-like K(+) channel. J. Neurogenet. *20*, 41-66.

Yu, Y.V., Bell, H.W., Glauser, D.A., Goodman, M.B., Van Hooser, S.D., and Sengupta, P. (2014). CaMKI-dependent regulation of sensory gene expression mediates experience-dependent plasticity in the operating range of a thermosensory neuron. Neuron *84*, 919-926.

Zhao, P., Zhang, Z., Ke, H., Yue, Y., and Xue, D. (2014). Oligonucleotide-based targeted gene editing in *C. elegans* via the CRISPR/Cas9 system. Cell Res. *24*, 247-250.

Click here to access/download

Supplemental Movies & Spreadsheets

TakeishiYu_Movie1.avi

Click here to access/download

Supplemental Movies & Spreadsheets

TakeishiYu_AWB_Movie2.avi

Click here to access/download

Supplemental Movies & Spreadsheets

TakeishiYu_Movie3.avi

Click here to access/download

Supplemental Movies & Spreadsheets

Takeishi_Yu_TableS2.xlsx